Chemical Engineering Journal 453 (2023) 139918

Contents lists available at ScienceDirect

Chemical Engineering Journal

journal homepage: www.elsevier.com/locate/cej

An interfacial gas-enrichment strategy for mitigating hydrate adhesion and blockage

Rui Ma, Senbo Xiao *, Yuanhao Chang, Yuequn Fu, Jianying He, Zhiliang Zhang *

NTNU Nanomechanical Lab, Department of Structural Engineering, Norwegian University of Science and Technology (NTNU), Trondheim 7491, Norway

ARTICLE INFO

Keywords:
Intermediate layer
Adhesion
Hydrate
Gas
Surface design

ABSTRACT

Unwanted gas hydrates blockage is a threat to the safety of oil–gas pipeline systems. Deploying passive anti-hydrate surfaces is a promising approach to circumventing the long-lasting hydrate problem, and a precise understanding of the interactions between hydrate and solid surfaces is a prerequisite for the creation of such surfaces. In this work, the underlying mechanisms and the key influencing factors of hydrate adhesion are explored by large-scale molecular dynamics simulations. Hydrates with an intermediate layer (IML) containing varied gas content are brought to contact with solid surfaces having different levels of wettability and roughness. It is found that the final IML structure is dictated by the gas concentration. Enriching gas content in the vicinity of solid surfaces is crucial for lowering hydrate adhesion strength. The results indicate that forming a molecular gas layer or gas bubbles on solid surfaces can enable the automatic detachment of the eventually formed hydrate on a pipeline wall surface under the action of shear flow. This study manifests our approach of utilizing an interfacial gas-enrichment strategy (IGES) for weakening hydrate adhesion as a novel passive anti-hydrate surface design.

1. Introduction

Natural gas hydrate, also called clathrate hydrate, is one special form of cage-like water crystal structure with trapped small guest molecules of methane, propane, carbon dioxide, hydrogen sulfide and others [1–4]. It has been widely found in permafrost and deep-water sediments and is believed to account for total carbon storage more than twice that of traditional oil and gas resources [5–8]. Therefore, the rational and safe exploration of gas hydrate resources is of great significance for alleviating the energy crisis and optimizing energy sources.

Undesirably, gas hydrates can also be found in the pipeline systems for transporting deep-water oil and gas resources. The formation and deposition of gas hydrates in pipelines often occur under special temperature and pressure conditions, which may lead to catastrophic consequences in flow assurance [9–13]. The nucleated hydrate particles in the moving multiphase fluid in pipelines inevitably collide with the pipe wall, hence followed by hydrate deposition in special areas [14–17]. Subsequently, the deposition of hydrates on the pipe wall induces hydrate growth, which reduces the inner diameter of the pipelines over time and drastically affects fluid flow velocity and flux in the pipeline [14,18]. In the last and final disastrous state, the formed hydrate bulk blocks the whole pipeline and induces extraordinarily high internal pressure, resulting in severe safety and leakage risks [19].

Hydrate nucleation requires a special condition of a gas and water phase coexistence [20–23]. Hydrate is unlikely to nucleate directly on solid surfaces [20,23,24]. Furthermore, it is proven that the whole process of hydrate nucleation is not affected by solid surfaces [21]. All these previous studies indicate that hydrate particles from flowing multiphase liquids are a widespread source of deposits on pipe walls. The deposition process of hydrates can usually be divided into the following two steps:

i. Hydrate particles migrate and contact solid surfaces. This step is often described as a hydrate particle with a pre-melted layer (or called quasi-liquid layer, QLL) in contact with solid surfaces (water film may exist on the surfaces) by capillary action [25–27]. It is noted that the QLL on hydrate particles can facilitate its adhesion even without a pre-existing water film to the pipeline surface. This formed intermediate layer (IML) between hydrate particle and solid surface greatly affects the hydrate adhesion behavior and performance. At this stage of hydrate deposition, the formed liquid bridges and the Laplace pressure through capillary action determine the strength of the adhesion.

* Corresponding authors.
E-mail addresses: senbo.xiao@ntnu.no (S. Xiao), zhiliang.zhang@ntnu.no (Z. Zhang).

https://doi.org/10.1016/j.cej.2022.139918
Received 25 July 2022; Received in revised form 2 October 2022; Accepted 16 October 2022
Available online 21 October 2022

ii. Solidification takes place under suitable conditions. If the contacts between a hydrate particle and a solid surface occur under the conditions of water condensation, namely in the appropriate temperature and pressure range for the formation of hydrate or ice, further solidification can be initiated [27]. The IML can thus be transformed into a solid phase, leading to the replacement of capillary action by solid bridging as confirmed by previous experiments [26,28].

Functional design of pipeline surfaces can be more economical and environmentally friendly than traditional hydrate plugging mitigation that uses chemicals or active heating [29–36]. Passive anti-hydrate surfaces that require no external force or energy inputs for realizing both deposition-suppressing and super-low hydrate adhesion can be the ultimate solution for hydrate blockage in pipelines. Embracing the knowledge in anti-icing, hydrophobic or superhydrophobic materials and designs have been proposed to reduce adhesion of hydrate [37–44]. Despite their similar appearance and density, the formation and decomposition of gas hydrate are to a great extent different from those of ice [45]. Because the two components of hydrate, namely water and gas molecules, have distinct molecular properties, hydrate formation requires a strong driving force to break the phase interface between water and gas for mass transfer [20,22,46]. Meanwhile, hydrate decomposition occurs spontaneously and rapidly under ambient conditions due to phase separation of water and gas molecules. Hypothetically, enhancing water–gas phase separation, or weakening the driving force for mass transfer across phase interface is an effective approach for inhibiting hydrate nucleation and reducing hydrate adhesion. The underlying mechanisms and kinetic process of such adhesion-solidification as well as the key factors determining the adhesion strength between hydrate particles and solid surfaces remain unexplored. In this work, the adhesion-solidification process of a hydrate particle on solid surfaces is studied by Molecular Dynamics (MD) simulations, with a focus on the structural evolution of the intermediate layer between hydrate and solid surfaces. The results resolve the relationship between hydrate adhesion strength and its interfacial atomistic structures, seeding an interfacial gas-enrichment strategy (IGES) for lowering the adhesion and shedding new light on passive anti-hydrate surface design.

2. Modeling and methods

2.1. Model systems for hydrate adhesion-solidification process

The hydrate adhesion-solidification process is modeled as a three-part system consisting of a prebuild hydrate lattice, IML, and a solid surface (Fig. 1). A detailed description of the modeling scenario is given in Section A in Supplementary. A standard prebuilt sI-structure hydrate with a volume of 4 × 4 × 3 lattices (2208 water molecules and 384 guest molecules) as the top layer of the system, capturing the atomistic features of hydrate particles. The IMLs with an initial thickness of ~ 5 nm in all the systems contain the same number of 4600 water molecules, but 5

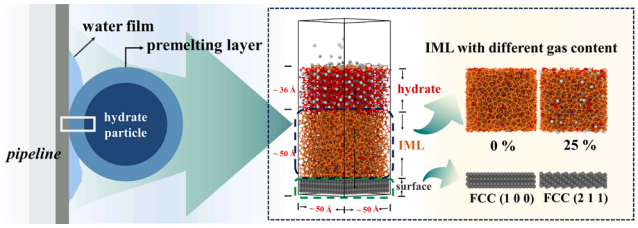

Fig. 1. Schematic of the simulation systems. The solid surface is shown as dark gray balls, guest molecules as white balls, amorphous water as orange sticks, and hydrate cage as red sticks. The color scheme applies to all snapshots in the following figures. The simulation box of the system is indicated by black framework. (For interpretation of the references to color in this figure legend, the reader is referred to the web version of this article.)

different gas concentrations of 0 %, 25 %, 50 %, 100 %, and 200 %. Here, the water-guest ratio in standard sI hydrate (4600 water molecules and 800 guests) is taken as 100 % gas concentration. The IMLs model accounts for a wide range of non-gas to super-saturated gas concentration situations. The chosen initial IMLs thickness in this work is sufficient to realize the hydrate adhesion-solidification process [47]. A solid surface with an FCC lattice structure is modeled as the bottom layer of the systems. Two representative solids surface types, termed S1 (lattice constant a1 = 3.649 Å) and S2 (lattice constant a2 = 4.158 Å), are chosen for the substrates [48]. In order to explore the effects of surface wettability, these two substrates have varied atomistic interaction strength with water in the system (Section B in Supplementary, Table S1) representing the surface wettability effect. Furthermore, both (1 0 0) and (2 1 1) crystal planes of each substrate are used for evaluating the possible lattice roughness effects in the final IML structure. Therefore, 4 surface models are used in this study, termed S1(1 0 0), S1(2 1 1), S2(1 0 0) and S2(2 1 1), respectively. All the surfaces have a similar apparent area of ~ 25 nm^2.

As schematically shown in Fig. 1, the simulation box in all the systems has periodic boundary conditions, and a vacuum buffer separating atomistic interactions between the top of hydrate and the solid substrate.

2.2. Force-fields and atomistic parameters

The interactions of water molecules are described by the monatomic water model mW [49]. This water model uses the three-body Stillinger–Weber (SW) potential to account for angle-dependent inter-atomic interactions in water, featuring hydrogen bonding [50]. The three-body interactions among the water molecules can correctly capture the tetrahedron structures of the hydrogen bonding network, which is crucial in the studies of hydrate and ice [51–57]. The guest molecules are described by the so-called "M" particle model, which is widely used to simulate small guest molecules, especially methane in hydrate [51,52]. The "M" particle interacts with other particles through the two-body SW potentials. The solid surface is fixed in position throughout the course of all the simulations. For the sake of simplicity, atoms in the solid surface only interact with water and gas via Lennard-Jones potential, with varied interaction strengths representing different surface wettability [23,48]. The corresponding detailed interaction parameters are given in Table S1 in the Supplementary.

2.3. Simulation setting of achieving hydrate adhesion-solidification process

All the MD simulations, including the adhesion-solidification process and the subsequent tensile test, are carried out using the LAMMPS (Large-scale Atomic/Molecular Massively Parallel Simulator) package [58]. All the systems are first subjected to energy minimization of the initial atomistic structure, followed by 1 ns equilibration for structural relaxation of the IML at 270 K. During the structural relaxation of the IML, the pre-built hydrate layer is fully immobilized. Due to the relatively high temperature of 270 K, the IML is expected to establish harmonized interactions with the hydrate and the surface, guaranteeing stable initial simulation systems for the subsequent IML solidification process.

All the systems used for hydrate adhesion-solidification process are then quenched to long equilibration at 210 K in the NVT ensemble. This temperature is chosen the same as in the previous studies to reproduce the hydrate and ice structures in the initial water layer with a comprehensive consideration of the molecular models, the water phase structure and the computational cost [48,51]. A Nose-Hoover thermostat is used for temperature control, with a coupling constant of 0.1 ps [59,60]. The time step in all the simulations is 10 fs. At least five independent runs (ten times for the pure water case) are performed for the IML solidification process in each system with simulation time of 200 ns. The

system properties are monitored and recorded during the whole simulation. The final system snapshots at the end of the simulations are then collected for the tensile testing of hydrate adhesion.

2.4. Tensile test of hydrate adhesion

The force applied onto macroscopic hydrate in pipelines by gas or flow fluid is highly complex, which is challenging to capture using only atomistic modeling. In the detaching event of hydrate from its adhesion surface, breaking of the atomistic contacts at the adhesion interface is the first and key step. As such, the modeling of this study is to focus on capturing the initial separation of hydrate from substrates by using tensile testing. In order to study the adhesion strength of hydrate, the pre-built hydrate layer in the systems is subjected to tensile pulling force by a moving harmonic spring to realize the tensile test, as the same approaches in previous studies [45,61]. A harmonic spring with a force constant of 1 kcal/mol/Å^2 is attached to the centre of mass of the pre-built hydrate and is set to move away from the immobilized solid surface. A constant moving speed of 0.001 Å/fs is used. By doing so, the stretched harmonic spring applies a tensile force onto the hydrate to enable its separation from the solid surface. The force profile of the harmonic spring is monitored. The pulling force is constantly increasing until a sudden drop occurs signifying the hydrate fracture from the solid surface. All the tensile tests stop when the detachment of the hydrate happens. The hydrate adhesion strength is calculated by taking the highest pulling force recorded normalized by the initial surface area of the solid surface. Because all the tensile tests use the same spring pulling speed, the results obtained are comparable for evaluating the difference in adhesion strength [62].

3. Results and discussion

3.1. Solidification of IML on different surfaces

The structure of the IML significantly affects the hydrate adhesion [45]. The evolution of the IML structure in each system during the solidification process is determined by various parameters, including gas content, surface wettability, roughness, and others. In addition, the wettability of the hydrate interface itself also has a significant impact on its evolution and structure [30,63–65], which is mainly reflected in the migration, adsorption and arrangement of water and gas molecules. For characterizing the IML structures, the Chill + algorithm is employed to identify the hydrate crystal structures in the water molecules [66]. Following the same approaches in previous studies [22,55], the number of water molecules in the hydrate crystal structure ($N_{hydrate}$) is taken as the size of hydrate in each system, as shown in Fig. 2.

The IML in each system indeed shows clear structural evolution during the solidification process, as indicated by direct comparison between the initial (t = 0 ns) and final (t = 200 ns) system snapshots (Fig. 2). There is an obvious top-down growth of hydrate crystal structure in the IML, indicating that the pre-built hydrate layer serves as a precursor of crystal structure seed. Except for one simulation sample containing 25 % guest molecules in the S1(1 0 0) system (Supplementary, section C), all the IMLs containing guest molecules are gradually transformed into cage structures of hydrate during the solidification process, disregarding the gas content. Interestingly, the IMLs containing only water molecules mostly form ice structures during the solidification, except those systems with the solid surface S2 (1 0 0) (Fig. 2b). It is important to note that the ice nucleates always on the solid surface (heterogeneous nucleation) and grows towards the pre-built hydrate layer, namely a bottom-up ice growth direction, which is opposite to the hydrate growth direction in other systems. Because these systems have no gas molecules contained in IML, the ice nucleation and growth solely result from the interaction between the surface and water molecules in the IML. The difference of the systems in initiating ice formation is highly reproducible, as confirmed by 10 independent runs of each simulation. Without gas molecules, there is an obvious competition between hydrate top-down growth and ice bottom-up growth in the IML (Supplementary, section D). For the surface of S1(1 0 0), S1(2 1 1) and S2 (2 1 1), ice growth starting from the surface dominates, consistent with previous studies [48]. For the special case of the S2(1 0 0), the combined effects of interactions between the surface with the water molecules, lattice arrangement and the surface roughness have delayed the ice nucleation and caused the full hydrate formation in the IML instead. This interesting phenomenon implies that templating crystal formation and control of the IML structure can be achieved through surface structural design, which can be an interesting future subject for investigation.

The presence of guest gas molecules in IML always enhances the formation of hydrate structures in the IML, in line with the known stabilizing effect of guest molecules on the hydrate cage structure [22,67,68]. A higher concentration of gas molecules results in faster hydrate growth in the IML, as shown in the monitored hydrate crystal

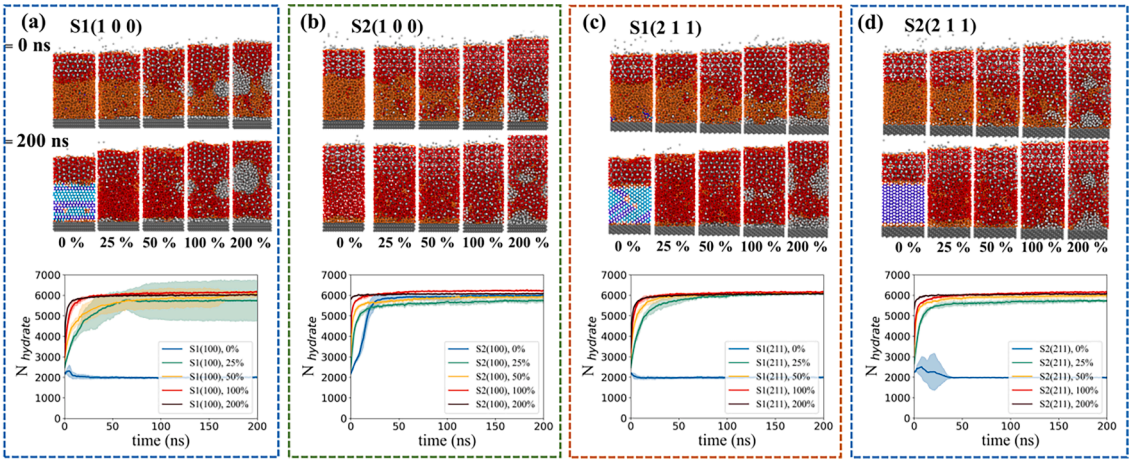

Fig. 2. Solidification of IML with varied gas content on different surfaces. The four surfaces are labeled in each system as (a) with S1(1 0 0), (b) with S2 (1 0 0), (c) with S1 (2 1 1) and (d) with S2(2 1 1). The initial (t = 0 ns) and final (t = 200 ns) system snapshots are given in the figure for the comparison of IML structure before and after the solidification. The light and dark blue sticks are used to distinguish cubic and hexagonal ice identified by the Chill + algorithm respectively, and the color scheme also applies to all following pictures. The evolution of hydrate crystal sizes represented by the number of water molecules in hydrate ($N_{hydrate}$) in the systems is given in the plots. Mean value of the raw data is shown as a solid color line, with the corresponding standard deviations of all independent runs given as similar faded colors. The legends give the content of the gas in the IML. (For interpretation of the references to color in this figure legend, the reader is referred to the web version of this article.)

size profiles during the simulation in Fig. 2(a-d). Different gas molecule content and distribution also result in different final solidified IML structures. Due to the heterogeneity of gas molecular spatial distribution, the final hydrate structure in the IML tends to be composed of many smaller filled and empty hydrate cage clusters with random orientations. These structures, especially the empty cages, agree with previous studies on the effect of the mass-transfer-limited process [69]. That is, the solidified water structure such as hydrate limits the gas mass transfer to fill the newly formed cages. Particularly, the IML with saturated (100 %) and supersaturated (200 %) gas molecules form obvious gas bubbles alongside the hydrate structure (snapshots, Fig. 2a-d). Depending on the wettability of the solid surface, the gas bubble can be trapped in the hydrate structure or dwell on the solid surface (forming a gas adsorption layer). Because surface S2 is more hydrophilic than S1, the final solidified IMLs in S2 adsorb more water molecules adjacent to the surface than those in S1, regardless of either on (1 0 0) or (2 1 1) faces. The high hydrophilicity of S2 also results in the exclusion of the gas molecule adjacent to the surface by water molecules, which is a driving force for gas bubble formation. In comparison, the lower hydrophilicity of S1 results in gas molecules dispersing more evenly on the surface, forming a gas adsorption layer. These differences in the composition and structure of the IML profoundly affect interface mechanical properties, which are studied by the subsequent tensile tests.

3.2. Tensile test to determine hydrate adhesion strength on solid surfaces

Tensile tests are carried out to determine the hydrate adhesion strength. With increasing pulling force, the hydrate layer with the IML is finally detached from the solid surface, as system snapshots are shown in Fig. 3. Here, all the water molecules in the hydrate and IML are completely detached from the solid surface, meaning the adhesion failure occurs at the IML-solid interface. It is worth noting that only the pre-built hydrate layer is directly subjected to the pulling force. The fully dewetting of water molecules in both the hydrate layer and the IML from the solid surfaces results from the strong non-bonded interactions among the water molecules, namely the hydrogen bonding network, which agrees with the previous nanoscale de-icing simulation results [61].

In comparison to the water molecules, the guest gas molecules in the IML have relatively weak interactions, which leads to residual gas molecules on the solid surfaces after the detachment (system snapshots, Fig. 3). The number of residual gas molecules remaining on the surfaces depends on the concentration of gas molecules in the IML and the wettability of the solid surface. Generally, higher gas concentration leads to more residual gas molecules, because of the higher possibility of gas molecules being excluded from the solid surface during the top-down hydrate growth process. It is surprising that the amount of residual gas molecules is also affected by surface wettability, as fewer residual gas molecules are found on surface S2 than S1. That is to say, fewer residual gas molecules are found on more hydrophilic surfaces. Remarkably, no residual gas was observed on S2(1 0 0) with IML containing 25 % and 50 % guest gas molecules. The guest gas molecules in these two systems are excluded away from the surfaces by a dense layer of water molecules owing to the hydrophilicity of S2(1 0 0). Gas molecules are completely encapsulated inside the hydrate structure formed during IML solidification. In systems with saturated and supersaturated gas concentrations in IMLs, residual gas molecules on the surfaces are always found due to water–gas phase separation and volume exclusion of the top-down hydrate growing front.

The adhesion strength of the IML is indeed greatly affected by the final solidified IML structure. As depicted by the force profiles in Fig. 3, the highest adhesion forces are observed for systems with IMLs of pure ice (IMLs with 0 % gas content in Fig. 3a, c and d). In sharp contrast, the highest adhesion force obtained in systems with IML of hydrate structure features a roughly 50 % decrease (IMLs with 0 % gas content in Fig. 3b), as confirmed by multiple independent runs shown in Supplementary Figure S4. This observation is consistent with results from previous studies, namely pure ice structure has nearly double adhesion strength on solid surfaces as that of hydrate structure without trapped gas molecules [45]. The adhesion strength of hydrate decreases with the increase of gas content in the IML, as confirmed by force profiles in Fig. 3 and Supplementary Figure S4. Considering the residual gas on the surfaces discussed above, the hydrate adhesion strength is determined by the molecular composition and local structure adjacent to the solid surfaces. The changes in the distribution of different molecules, especially gas molecules, greatly affected the adhesion of hydrate on solid surfaces. For gas content higher than 200 % in the IML not modeled in this work, hydrate adhesion strength is thus expected to further decrease.

3.3. The effect of surfaces wettability on gas and hydrate adhesion

The gas content in the IML has shown a profound impact on hydrate adhesion (Fig. 3). The distribution of gas molecules in the solidified IML, especially those adjacent to the solid surface, yet is determined by the surface wettability. It is thus important to decipher the complex relationship between surface wettability and the resulting molecular composition and structure of the IML, and further with the corresponding hydrate adhesion strength.

The adjacent molecular layer to the solid surface directly influences hydrate adhesion strength. As summarized in Fig. 4(a), high gas content in the IML leads to low hydrate adhesion strength in all the systems. There are six typical patterns of adjacent layers of molecules to the solid surfaces observed, as shown in Fig. 4(b). Water film adjacent layer is

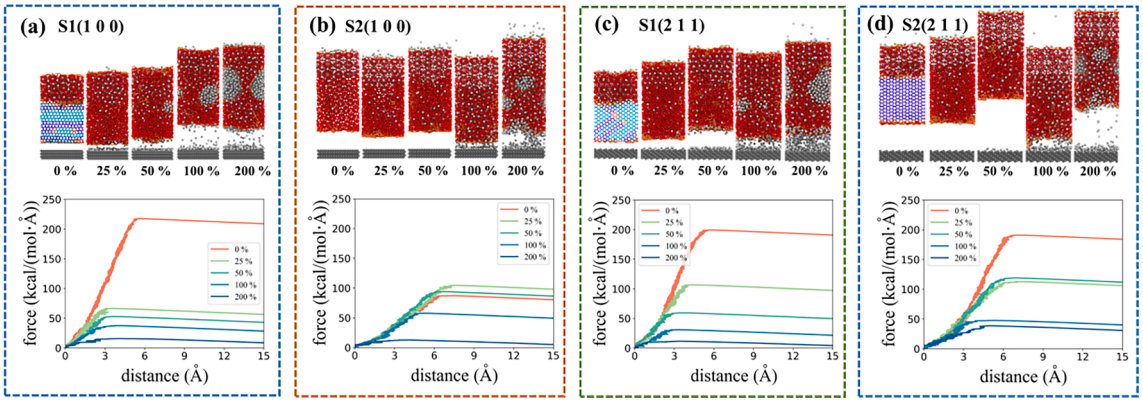

Fig. 3. Tensile test of hydrates on the four solid surfaces. (a) S1(1 0 0), (b) S2(1 0 0), (c) S1(2 1 1) and (d) S2(2 1 1). Representative system snapshots are included with the hydrate layer and the solidified IML right after being detached from the solid surfaces. Characteristic force profiles monitored during the tensile testing on each surface are plotted with legends showing the gas content in the IML.

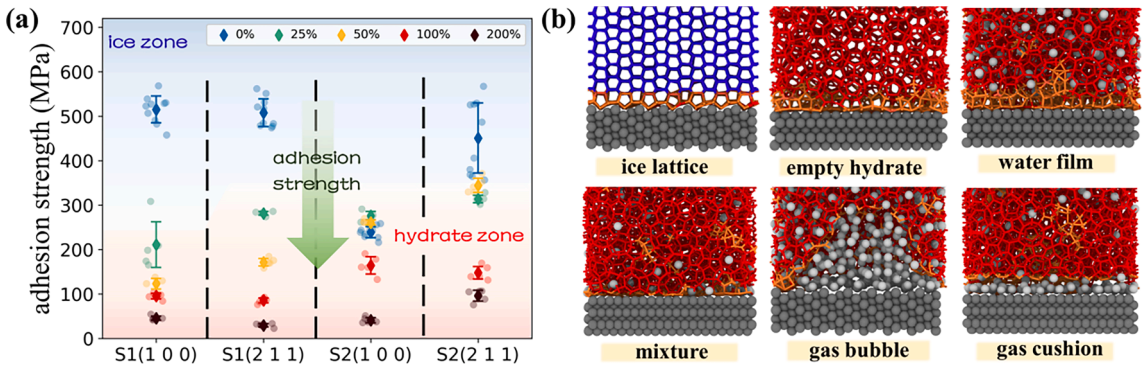

Fig. 4. Hydrate adhesion strength and the underlying adjacent molecular layer to the solid surfaces (a) Adhesion strengths of various IML on different solid surfaces. Hydrate adhesion strengths obtained from IMLs with the same gas content share the same color in the plot. The raw data are shown in spherical dots, while the mean values are shown in diamond dots with an error bar indicating the standard deviation. Each sample point in the ice zone means that at least one stable ice cluster formation is observed in the corresponding simulated trajectory. (b) Six typical adjacent molecular layer patterns of ice lattice, empty hydrate, water film, mixture, gas bubble and gas cushion, are observed in the systems.

commonly observed on relatively more hydrophilic surfaces (type S2) with lower gas content (empty hydrate pattern also contains similar water film at the IML-solid interface, Fig. 4(b)). In cases of supersaturating gas content in the IML, the adjacent layer on more hydrophilic surfaces often contains a gas bubble generated during the solidification process of the IML. On less hydrophilic surfaces (type S1), gas cushion adjacent layer is common monitored. For the systems forming ice in IML, the adjacent layer has an ice-like lattice structure. Overall, pure ice lattice adjacent layers associate with the highest hydrate adhesion strengths, while adjacent layers of water film, mixture, gas bubbles and gas cushion lead to sequentially lowered hydrate adhesion strength. Such order indicates that hydrate adhesion strength decrease with increasing interfacial gas content. When the multi-layer gas adsorption is formed on the interface, the IML-solid interface will transform into a gas interface, resulting in minimum adhesion strength. Given that pressure could also potentially alter the final structure of the IML, an additional set of IML solidification simulations under pressure of 100 bar are performed. The evolution process and the final pattern of the interfacial layer under pressure are found to be consistent with the above models without pressure. These new simulations further confirm the significance of the results of IML formation. Detailed information on the simulations under pressure is provided in Section F of the Supplementary Materials.

It is important to highlight the role of the surface wettability, namely the relative affinity of gas or water molecules to the surface, in the formation of the different adjacent molecular layers. Specifically, a high percentage of gas molecules in the adjacent molecular layer favors low hydrate adhesion strength, which is yet restricted by high surface hydrophilicity for the propensity of accumulating adjacent water films. The most obvious example of such a competing effect is exhibited by the similar adhesion strengths monitored on the S2(1 0 0) with 0 %, 25 % and 50 % gas content in the IML (Fig. 4a). Increasing gas content in the IML does not result in decreasing adhesion strength in these three systems, because the high surface hydrophilicity of S2(1 0 0) leads to the same tightly bound water adjacent layers. A similar example can be seen on the S2(2 1 1) surface with IML containing 0 %, 25 % and 50 % gas molecules, despite that S2(2 1 1) can trigger ice formation in the IML with 0 % gas content and result in even higher ice adhesion strength. For systems with high gas content in the IML (100 % and 200 %), the surface wettability effect on the hydrate adhesion strength is less pronounced. In these systems, hydrate adhesion strength monitored is generally low due to the weak interactions of the gas molecules in the adjacent molecular layer. Nevertheless, the high hydrophilicity of the S2(2 1 1) surface can still lock a few water molecules in the adjacent molecular layer in the case of IML with 200 % gas content, resulting in gas bubble and slightly higher hydrate adhesion strength than those with pure gas cushion layers (Fig. 4a). For surface S1, the relatively low surface hydrophilicity always results in gas cushion adjacent layer, and subsequently low hydrate adhesion strength. It is worth noting that surface roughness can also enhance hydrate adhesion. The atomistic rougher surface (2 1 1) plane yields slightly higher hydrate adhesion strength than the surface (1 0 0), given the same adjacent molecular layer.

3.4. The effect of surfaces wettability on the interfacial water

Without gas molecules in the adjacent molecular layer, amorphous water film and ice lattice clearly lead to varied adhesion strength. Further elucidating the relationship between surface wettability and the structures of IML without gas is yet another important step for understanding the interaction of hydrates with solid surfaces.

Given that the smooth (1 0 0) lattice face can allow either ice or hydrate formation in the IML (S1(1 0 0) and S2(1 0 0) in Fig. 2a and 2b), water freezing process on the same surface is further explored with varied surface hydrophilicity. Specifically, pure water freezing simulations are carried out on surfaces with varied interaction strength (ε_{ws}) at three temperatures of 210 K, 220 K and 230 K, as shown in Fig. 5. The adjacent layer of the water molecules on the solid surface is then characterized for the total molecule number and its structure.

There is a linear correlation between water contact angle on smooth/flat surfaces and adhesion strength of ice – the lower the adhesion strength of ice on a more hydrophobic solid surface [70,71]. Our atomistic simulations also show the same results at the nanoscale, the number of water molecule changes in the adjacent layer affected by the surface hydrophilicity is shown in Fig. 5(a). Decreasing surface ε_{ws}, namely increasing surface hydrophobicity, results in decreasing water molecules in the adjacent layer on the solid surface at different temperatures. Such a trend in water molecule distribution on the surfaces is further confirmed by the radial distribution function (RDF) of water molecules from solid surfaces, as shown in Fig. 5(b). The height of the first peak in the RDF profiles decreases with the decrease of the ε_{ws} value. The result indicates that lower ε_{ws} lead to a looser adjacent water layer. Interestingly, surfaces with higher ε_{ws} values also have a higher probability of ice formation in the IML. At 210 K, ice formation is observed on all the surfaces except in a few cases with low ε_{ws} (Fig. 5a). At a relatively higher temperature of 220 K, ice forms only on surfaces with high ε_{ws} values. It is clear from the result that temperature also has a significant effect on the final structure of the IML, namely determining formation of ice or amorphous water structures. Nevertheless, the pattern of linear decrease in the amount of interfacial water with the increase of surface hydrophobicity is consistent. As discussed above, in the absence of pre-existing hydrate and guest molecules, there is no observation of the transformation of amorphous water into hydrate

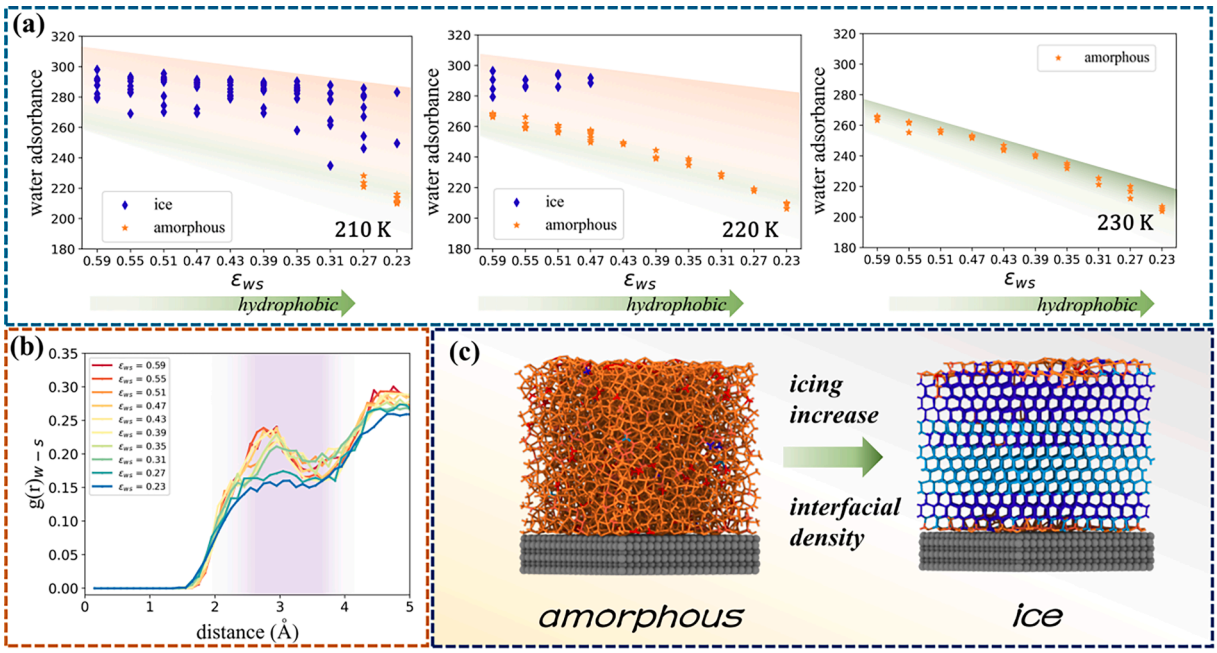

Fig. 5. Influence of surface hydrophobicity on water molecules close to solid surfaces. (a) The number of water molecules in the adjacent layer on surfaces with varied surface interaction strength ε_{ws} at different temperatures. (b) Radial distribution functions (RDF) of water molecules on surfaces with varied ε_{ws}. (c) Comparison of water structure before and after icing occurs. Icing increases the areal density of water molecules adjacent to the surface.

water cages and no further competitive growth of top-down hydrate and bottom-up ice in the IML. Therefore, delayed ice formation on surfaces facilitates the transformation of IML to hydrate structures, and thus lowers hydrate adhesion strength. It should be noted that formation of ice always leads to an increase in the number of water molecules in the adjacent water layer to the solid surfaces with the same ε_{ws} (Fig. 5c). The increasing number of water molecules or the increased spatial distribution density of water in the adjacent layer is the molecular origin underpinning the elevated adhesion strength of the water structure on the solid surface.

3.5. Interfacial gas-enrichment strategy (IGES) for lowering hydrate adhesion

The above results indicate that enrichment of gas in the adjacent molecular layer on solid surfaces can significantly weaken the surface wettability-controlled hydrate adhesion strength. Considering that gas bubbles were often found on solid surfaces in previous experimental studies [72–75], it is rational to take the maximization of gas content on solid surfaces as a practical strategy in the design of anti-hydrate surfaces, termed the interfacial gas-enrichment strategy (IGES). For quantifying surface performance following the design strategy depicted in Fig. 6(a), a crucial surface property, namely surface gas coverage (R_{gc}), can be defined:

$$R_{gc} = \frac{S_{gas}}{S_{hydrate}}$$

where $S_{hydrate}$ is the apparent contact area of hydrate particle deposition on solid surfaces, and S_{gas} is the area of the gas region on the same surface. Considering the hydrodynamic shear force generated from the oil/gas flow in pipelines, there should be a critical gas coverage (R_{cgc}) which enables hydrate automatic detachment from the solid pipe wall surface:

$$R_{cgc} = \frac{S^{c}_{gas}}{S_{hydrate}}$$

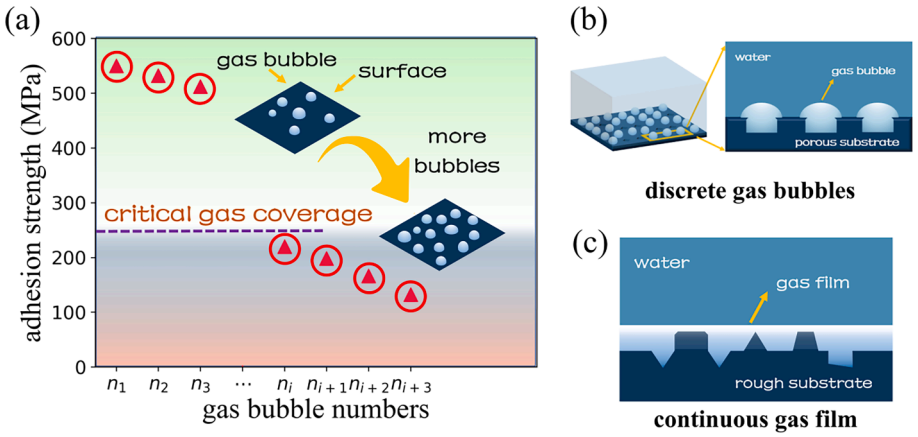

Fig. 6. Conceptual interfacial gas-enrichment strategy (IGES) for anti-hydrate surface design. (a) Schematic of surface gas coverage (R_{gc}) and critical gas coverage (R_{cgc}) for enabling automatic hydrate detachment. (b) Nanobubble-based approach to achieve IGES. (c) Schematic of hypothetical continuous gas film coverage.

Here, S^c_{gas} denotes the critical gas coverage on a specific solid surface for the automatic hydrate detachment. As such, hydrate adhesion strength, defined as shearing stress (τ) similar to previous anti-icing studies [40], should be reversely correlated with R_{gc} on different surfaces. For the realization of spontaneous hydrate detachment, a surface should then enable the critical shear strength (τ_c) lower than the shearing stress applied by the flowing fluids in pipelines. In practice, τ_c depends on the material properties of the solid surfaces, namely R_{cgc}, as well as the fluid properties and dynamics of the flow, which should be quantified in different pipelines.

The proposed IGES can be realized by taking advantage of previous experimental observations, for example, the pinning effect [74,76] of nanobubbles underwater as shown in Fig. 6(b). Ideally, continuous or semi-continuous gas film on solid surfaces is the ultimate goal of anti-hydrate surfaces designed following IGES, as shown in Fig. 6(c). In such an idealistic situation, clean surfaces or always dry pipeline wall can be achieved as the solution to the hydrate blockage problem. It is important to highlight the contradictory conclusions derived from various studies on the hydrate promotion by gas bubbles on solid surfaces. Some studies indicate gas bubbles can promote hydrate formation under specific conditions depending on surface morphology and curvature of the nanobubbles [20,46], while others suggest otherwise [20,21,24]. The contradictory results certainly need further in-depth investigations. Nevertheless, high gas content on solid surfaces hindering hydrate adhesion strength, namely the basis of the IGES, is valid for the realization of automatic hydrate detachment in anti-hydrate surface design.

There are clear advantages in adopting IGES for anti-hydrate surfaces, for example, the greatly reduced hydrate adhesion strength resulting from the adjacent gas-rich layer, the inhibition of ice formation and prevention of resulting super-strong adhesion, the replenishable gas molecules from the flow in the pipeline without extra chemicals, just to name a few. The key of the proposed interfacial gas-enrichment strategy does not rely on the gas flow onto the surface after hydrate formation, but rather on the surface wettability. The concept of IGES contains the control of surface wettability as an important approach for surface design, indicating hydrophobic or superhydrophobic materials can be good candidates for anti-hydrate surfaces. New materials solutions following the IGES can be realized starting from those already available in experimental testing [77–79], which is subjected to the next steps of this study.

3.6. Interpretation of roughness effects on gas accumulation

Rough surface structures have potential in gas accumulation for lowering hydrate adhesion. It is known that superhydrophobic surfaces with hierarchical structures for the Cassie-Baxter wetting state have a great capacity for surface gas storage [77,78,80–82]. However, the hierarchical structures of superhydrophobic surfaces are known to suffer from insufficient durability, which could be vital to the application of anti-hydrate inside pipelines [83–85]. Given that a fraction of gas molecules for constructing the adjacent molecular layer on solid surfaces is already significant for reducing hydrate adhesion, hierarchical surface roughness might not be a prerequisite for IGES. As shown in Fig. 7, an increase in the true surface area of solid surfaces results in an increase in gas content in the adjacent molecular layer. The (211) surface plane is rougher than the (100) plane, and thus larger true surface area. The capacity gain due to the increase in the true surface area is non-linear for gas and water molecules and is more conducive to gas accumulation. For the same given number of water molecules in the adjacent molecular layer, there are generally more gas molecules in the adjacent layer on the (211) plane than on the (100) plane, as shown in Fig. 7(a). It is expected that such a phenomenon is even more obvious on surfaces with higher hydrophobicity, as water molecules need to sacrifice the chances of forming hydrogen bonds with other water molecules to stay on the surface. For the specific (211) plane roughness, gas molecules are thus more likely to be found in the grooves of the lattice plane, as shown in Fig. 7(c). The increasing population of gas molecules (decreasing of water molecules) on both (100) and (211) plane of the S1 and S2 surface ultimately leads to gas adjacent layer and fatally weakens hydrate adhesion (Fig. 7b).

4. Conclusions

In this work, the solidification of the intermediate layer (IML) with varied gas content is investigated by molecular dynamics simulations. The solidified IML structure is strongly correlated to the solid surface properties and the gas concentration. By applying a tensile force to quantify the adhesion strength of hydrate, the results elucidate the importance of molecular composition and surface wettability to hydrate adhesion strength. The results show that both hydrate and ice can form in the IML, indicating delayed ice heterogeneous nucleation by surface design favors hydrate formation in the IML and subsequently lowers hydrate adhesion. It is found here that high gas content in the adjacent molecular layer on solid surfaces is crucial for low hydrate adhesion strength, which could be a viable mechanism for the design and fabrication of anti-hydrate surfaces. Particularly, an interfacial gas-enrichment strategy (IGES) is promoted for anti-hydrate surfaces, with a well-defined parameter of critical gas coverage (R_{cgc}) for realizing automatic hydrate detachment from the future anti-hydrate surfaces. How to realize the IGES for practical application is still an open question awaiting further experimental exploration. The results in this work seed the concept of utilizing gas molecules for weakening hydrate adhesion, which provides inspiration also for related studies on other low adhesion surfaces.

CRediT authorship contribution statement

Rui Ma: Conceptualization, Writing – original draft. **Senbo Xiao:** Validation, Software, Writing – review & editing. **Yuanhao Chang:** Methodology. **Yuequn Fu:** Software. **Jianying He:** Writing – review & editing. **Zhiliang Zhang:** Writing – review & editing, Supervision.

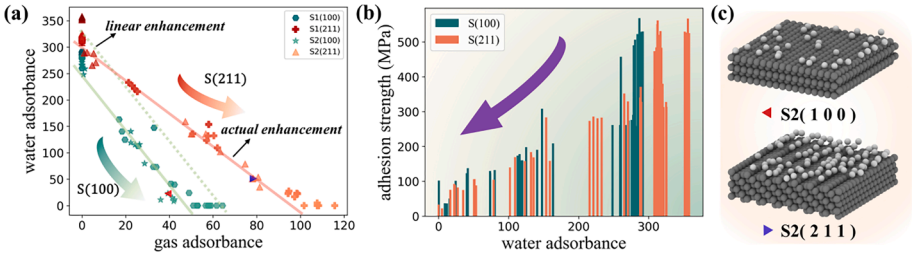

Fig. 7. Surfaces roughness effect on interfacial gas accumulation. (a) Gas and water molecule numbers in the adjacent molecular layer at the end of each simulation. Given the same number of water molecules in the adjacent molecular layer, surfaces with (211) plane tend to have more gas molecules. (b) Hydrate adhesion strength changes with the number of water molecules in the adjacent molecular layer. (c) Representative of gas molecule distribution after solidification on S2(100) and S2(211) with 100% gas content in the IML. More gas molecules are commonly monitored on (211) surfaces. Red and blue triangles in (c) mark the source of the snapshot in (a). (For interpretation of the references to color in this figure legend, the reader is referred to the web version of this article.)

Declaration of Competing Interest

The authors declare that they have no known competing financial interests or personal relationships that could have appeared to influence the work reported in this paper.

Data availability

No data was used for the research described in the article.

Acknowledgments

We are grateful for the support of the Research Council of Norway through the D'andra project (Project No. 302348). The supercomputer CPU hours were provided by the Norwegian Metacenter for Computational Science (Grant No. NN9110K, NN9391K, and NN8084K).

Appendix A. Supplementary data

Supplementary data to this article can be found online at https://doi.org/10.1016/j.cej.2022.139918.

References

[1] E.D. Sloan Jr, C.A. Koh, Clathrate hydrates of natural gases, CRC press2007.
[2] H.-J. Ng, D.B. Robinson, Hydrate formation in systems containing methane, ethane, propane, carbon dioxide or hydrogen sulfide in the presence of methanol, Fluid Phase Equilib. 21 (1–2) (1985) 145–155.
[3] Z.T. Ward, R.A. Marriott, A.K. Sum, E.D. Sloan, C.A. Koh, Equilibrium data of gas hydrates containing methane, propane, and hydrogen sulfide, J. Chem. Eng. Data 60 (2) (2015) 424–428.
[4] E.D. Sloan, Natural gas hydrates, J. Petrol. Technol. 43 (12) (1991) 1414–1417.
[5] Z.R. Chong, S.H.B. Yang, P. Babu, P. Linga, X.-S. Li, Review of natural gas hydrates as an energy resource: Prospects and challenges, Appl. Energy 162 (2016) 1633–1652.
[6] F. Li, Q. Yuan, T. Li, Z. Li, C. Sun, G. Chen, A review: Enhanced recovery of natural gas hydrate reservoirs, Chin. J. Chem. Eng. 27 (9) (2019) 2062–2073.
[7] K.A. Kvenvolden, Methane hydrate—a major reservoir of carbon in the shallow geosphere? Chem. Geol. 71 (1–3) (1988) 41–51.
[8] T.S. Collett, Energy resource potential of natural gas hydrates, AAPG Bull. 86 (11) (2002) 1971–1992.
[9] W. Prassl, J. Peden, K. Wong, Mitigating gas hydrate related drilling risks: a process-knowledge management approach. SPE Asia Pacific Oil and Gas Conference and Exhibition, Society of Petroleum Engineers, 2004.
[10] C.A. Koh, A.K. Sum, E.D. Sloan, Gas hydrates: Unlocking the energy from icy cages, J. Appl. Phys. 106 (6) (2009) 9.
[11] E.D. Sloan, Natural gas hydrates in flow assurance, Gulf Professional Publishing, 2010.
[12] M. Akhfash, Z.M. Aman, S.Y. Ahn, M.L. Johns, E.F. May, Gas hydrate plug formation in partially-dispersed water–oil systems, Chem. Eng. Sci. 140 (2016) 337–347.
[13] Z. Wang, Y. Zhao, B. Sun, L. Chen, J. Zhang, X. Wang, Modeling of hydrate blockage in gas-dominated systems, Energy Fuels 30 (6) (2016) 4653–4666.
[14] Z. Wang, J. Zhang, B. Sun, L. Chen, Y. Zhao, W. Fu, A new hydrate deposition prediction model for gas-dominated systems with free water, Chem. Eng. Sci. 163 (2017) 145–154.
[15] E.I. Jassim, M.A. Abdi, Y. Muzychka, A CFD-based model to locate flow-restriction induced hydrate deposition in pipelines, Offshore technology conference, OnePetro, 2008.
[16] Z. Liu, Z. Liu, J. Wang, M. Yang, J. Zhao, Y. Song, Hydrate blockage observation and removal using depressurization in a fully visual flow loop, Fuel 294 (2021), 120588.
[17] X. Zhang, B.R. Lee, J.-H. Sa, K.J. Kinnari, K.M. Askvik, X. Li, A.K. Sum, Hydrate management in deadlegs: effect of wall temperature on hydrate deposition, Energy Fuels 32 (3) (2018) 3254–3262.
[18] Z. Liu, Y. Li, W. Wang, G. Song, Y. Ning, X. Liu, J. Zhang, Investigation into the formation, blockage and dissociation of cyclopentane hydrate in a visual flow loop, Fuel 307 (2022), 121730.
[19] B. Shi, S. Song, Y. Chen, X. Duan, Q. Liao, S. Fu, L. Liu, J. Sui, J. Jia, H. Liu, Status of natural gas hydrate flow assurance research in China: A review, Energy Fuels 35 (5) (2021) 3611–3658.
[20] Z. He, P. Linga, J. Jiang, CH4 Hydrate Formation between Silica and Graphite Surfaces: Insights from Microsecond Molecular Dynamics Simulations, Langmuir the Acs Journal of Surfaces & Colloids (2017) acs.langmuir.7b02711.
[21] S. Cox, D. Taylor, T. Youngs, A.K. Soper, T.S. Totton, R.G. Chapman, M. Arjmandi, M.G. Hodges, N.T. Skipper, A. Michaelides, Formation of Methane Hydrate in the Presence of Natural and Synthetic Nanoparticles, J. Am. Chem. Soc. 140 (9) (2018) 3277–3284.
[22] L. Li, J. Zhong, Y. Yan, J. Zhang, X.C. Zeng, Unraveling nucleation pathway in methane clathrate formation, Proceedings of the National Academy of Sciences 117 (40) (2020).
[23] R. Ma, H. Zhong, L. Li, J. Zhong, Y. Yan, J. Zhang, J. Liu, Molecular Insights into the Effect of a Solid Surface on the Stability of a Hydrate Nucleus, The Journal of Physical Chemistry C 124 (4) (2020) 2664–2671.
[24] Z. He, F. Mi, F. Ning, Molecular insights into CO2 hydrate formation in the presence of hydrophilic and hydrophobic solid surfaces, Energy 121260 (2021).
[25] N.N. Nguyen, R.d. Berger, H.-J.r. Butt, Premelting-induced agglomeration of hydrates: Theoretical analysis and modeling, ACS applied materials & interfaces 12 (12) (2020) 14599-14606.
[26] N.N. Nguyen, R.d. Berger, M. Kappl, H.-J.r. Butt, Clathrate Adhesion Induced by Quasi-Liquid Layer, The Journal of Physical Chemistry C 125(38) (2021) 21293-21300.
[27] Z.M. Aman, E.P. Brown, E.D. Sloan, A.K. Sum, C.A. Koh, Interfacial mechanisms governing cyclopentane clathrate hydrate adhesion/cohesion, PCCP 13 (44) (2011) 19796–19806.
[28] Z.M. Aman, W.J. Leith, G.A. Grasso, E.D. Sloan, A.K. Sum, C.A. Koh, Adhesion force between cyclopentane hydrate and mineral surfaces, Langmuir 29 (50) (2013) 15551–15557.
[29] W. Ke, M.A. Kelland, Kinetic hydrate inhibitor studies for gas hydrate systems: a review of experimental equipment and test methods, Energy Fuels 30 (12) (2016) 10015–10028.
[30] L. Jiafang, Liu, Jinxiang, Wang, Xiaopu, Yan, Youguo, Zhang, Jun, The molecular mechanism of the inhibition effects of PVCaps on the growth of sI hydrate: an unstable adsorption mechanism, PCCP, Physical chemistry chemical physics, 2018.
[31] V.W. Lim, P.J. Metaxas, P.L. Stanwix, M.L. Johns, G. Haandrikman, D. Crosby, Z. M. Aman, E.F. May, Gas hydrate formation probability and growth rate as a function of kinetic hydrate inhibitor (KHI) concentration, Chem. Eng. J. 388 (2020), 124177.
[32] Y. Lu, C. Yuan, H. Wang, L. Yang, L. Zhang, J. Zhao, Y. Song, Atomistic insights into the performance of thermodynamic inhibitors in the nucleation of methane hydrate, Chem. Eng. J. 431 (2022), 133479.
[33] H.-J. Noh, D. Lee, W. Go, G. Choi, Y.-K. Im, J. Mahmood, Y. Seo, J.-B. Baek, Fused aromatic networks as a new class of gas hydrate inhibitors, Chem. Eng. J. 433 (2022), 133691.
[34] S. Gao, Hydrate risk management at high watercuts with anti-agglomerant hydrate inhibitors, Energy Fuels 23 (4) (2009) 2118–2121.
[35] C.N. Khalil, N.D.O. Rocha, L.C.F. Leite, Process for the thermo-hydraulic control of gas hydrates, Google Patents (2000).
[36] Y. Bai, Q. Bai, Subsea engineering handbook, Gulf Professional Publishing, 2018.
[37] L. Chenwei, W. Zhiyuan, T. Jinlin, Y. Ci, L. Mingzhong, Fundamental investigation of the adhesion strength between cyclopentane hydrate deposition and solid surface materials, Chem. Eng. Sci. 217 (2020), 115524.
[38] S. Dong, M. Li, C. Liu, J. Zhang, G. Chen, Bio-inspired superhydrophobic coating with low hydrate adhesion for hydrate mitigation, J. Bionic Eng. 17 (5) (2020) 1019–1028.
[39] F. Wang, R. Ma, S. Xiao, N.J. English, J. He, Z. Zhang, Anti-gas hydrate surfaces: perspectives, progress and prospects, J. Mater. Chem. A (2022).
[40] Z. He, S. Xiao, H. Gao, J. He, Z. Zhang, Multiscale crack initiator promoted super-low ice adhesion surfaces, Soft Matter 13 (37) (2017) 6562–6568.
[41] Y. Zhuo, V. Håkonsen, Z. He, S. Xiao, J. He, Z. Zhang, Enhancing the mechanical durability of icephobic surfaces by introducing autonomous self-healing function, ACS Appl. Mater. Interfaces 10 (14) (2018) 11972–11978.
[42] Z. He, Y. Zhuo, F. Wang, J. He, Z. Zhang, Understanding the role of hollow sub-surface structures in reducing ice adhesion strength, Soft Matter 15 (13) (2019) 2905–2910.
[43] Z. He, Y. Zhuo, F. Wang, J. He, Z. Zhang, Design and preparation of icephobic PDMS-based coatings by introducing an aqueous lubricating layer and macro-crack initiators at the ice-substrate interface, Prog. Org. Coat. 147 (2020), 105737.
[44] T. Li, P.F. Ibáñez-Ibáñez, V. Håkonsen, J. Wu, K. Xu, Y. Zhuo, S. Luo, J. He, Z. Zhang, Self-Deicing Electrolyte Hydrogel Surfaces with Pa-level Ice Adhesion and Durable Antifreezing/Antifrost Performance, ACS Appl. Mater. Interfaces 12 (31) (2020) 35572–35578.
[45] R. Ma, F. Wang, Y. Chang, S. Xiao, N.J. English, J. He, Z. Zhang, Unraveling Adhesion Strength between Gas Hydrate and Solid Surfaces, Langmuir 37 (47) (2021) 13873–13881.
[46] M.R. Walsh, G.T. Beckham, C.A. Koh, E.D. Sloan, D.T. Wu, A.K. Sum, Methane hydrate nucleation rates from molecular dynamics simulations: Effects of aqueous methane concentration, interfacial curvature, and system size, The Journal of Physical Chemistry C 115 (43) (2011) 21241–21248.
[47] D. Bai, G. Chen, X. Zhang, W. Wang, Microsecond molecular dynamics simulations of the kinetic pathways of gas hydrate formation from solid surfaces, Langmuir 27 (10) (2011) 5961–5967.
[48] M. Fitzner, G.C. Sosso, F. Pietrucci, S. Pipolo, A. Michaelides, Pre-critical fluctuations and what they disclose about heterogeneous crystal nucleation, Nat. Commun. 8 (1) (2017) 2257.
[49] V. Molinero, E.B. Moore, Water modeled as an intermediate element between carbon and silicon, J. Phys. Chem. B 113 (13) (2009) 4008–4016.
[50] F.H. Stillinger, T.A. Weber, Computer simulation of local order in condensed phases of silicon, Physical review B 31 (8) (1985) 5262.
[51] L.C. Jacobson, W. Hujo, V. Molinero, Nucleation pathways of clathrate hydrates: effect of guest size and solubility, J. Phys. Chem. B 114 (43) (2010) 13796–13807.
[52] L.C. Jacobson, V. Molinero, A Methane– water model for coarse-grained simulations of solutions and clathrate hydrates, J. Phys. Chem. B 114 (21) (2010) 7302–7311.

[53] B.C. Knott, V. Molinero, M.F. Doherty, B. Peters, Homogeneous nucleation of methane hydrates: Unrealistic under realistic conditions, J. Am. Chem. Soc. 134 (48) (2012) 19544–19547.
[54] A.H. Nguyen, L.C. Jacobson, V. Molinero, Structure of the clathrate/solution interface and mechanism of cross-nucleation of clathrate hydrates, The Journal of Physical Chemistry C 116 (37) (2012) 19828–19838.
[55] L. Lupi, A. Hudait, V. Molinero, Heterogeneous nucleation of ice on carbon surfaces, J. Am. Chem. Soc. 136 (8) (2014) 3156–3164.
[56] A.H. Nguyen, M.A. Koc, T.D. Shepherd, V. Molinero, Structure of the ice–clathrate interface, The Journal of Physical Chemistry C 119 (8) (2015) 4104–4117.
[57] M. Lauricella, G. Ciccotti, N.J. English, B. Peters, S. Meloni, Mechanisms and Nucleation Rate of Methane-Hydrate by Dynamical Nonequilibrium Molecular Dynamics, Journal of Physical Chemistry C (2017) acs.jpcc.7b05754.
[58] S. Plimpton, Fast parallel algorithms for short-range molecular dynamics, J. Comput. Phys. 117 (1) (1995) 1–19.
[59] W.G. Hoover, Canonical dynamics: Equilibrium phase-space distributions, Phys. Rev. A 31 (3) (1985) 1695.
[60] W.G. Hoover, Constant-pressure equations of motion, Phys. Rev. A 34 (3) (1986) 2499.
[61] S. Xiao, J. He, Z. Zhang, Nanoscale deicing by molecular dynamics simulation, Nanoscale 8 (30) (2016) 14625–14632.
[62] J. Wu, F. Ning, T.T. Trinh, S. Kjelstrup, T.J. Vlugt, J. He, B.H. Skallerud, Z. Zhang, Mechanical instability of monocrystalline and polycrystalline methane hydrates, Nat. Commun. 6 (1) (2015) 1–10.
[63] M.a.L. Martínez de Baños, N. Hobeika, P. Bouriat, D. Broseta, E. Enciso, F. Clement, R. Brown, How do gas hydrates spread on a substrate?, Crystal Growth & Design 16 (8) (2016) 4360-4373.
[64] A.A. Bertolazzo, P.M. Naullage, P. Baron, M. Valeria, The Clathrate-Water Interface Is Oleophilic, J. Phys. Chem. Lett. (2018) 3224–3231.
[65] H.M. Stoner, A. Phan, A. Striolo, C.A. Koh, Water Wettability Coupled with Film Growth on Realistic Cyclopentane Hydrate Surfaces, Langmuir 37 (42) (2021) 12447–12456.
[66] A.H. Nguyen, V. Molinero, Identification of clathrate hydrates, hexagonal ice, cubic ice, and liquid water in simulations: The CHILL+ algorithm, J. Phys. Chem. B 119 (29) (2015) 9369–9376.
[67] L.C. Jacobson, W. Hujo, V. Molinero, Thermodynamic stability and growth of guest-free clathrate hydrates: a low-density crystal phase of water, J. Phys. Chem. B 113 (30) (2009) 10298–10307.
[68] H. Zhong, L. Li, R. Ma, J. Zhong, Y. Yan, S. Li, J. Zhang, J. Liu, Two-dimensional hydrogen hydrates: structure and stability, PCCP 22 (10) (2020) 5774–5784.
[69] H. Liang, D. Guan, K. Shi, L. Yang, L. Zhang, J. Zhao, Y. Song, Characterizing mass-transfer mechanism during gas hydrate formation from water droplets, Chem. Eng. J. 428 (2022), 132626.
[70] A.J. Meuler, J.D. Smith, K.K. Varanasi, J.M. Mabry, G.H. McKinley, R.E. Cohen, Relationships between water wettability and ice adhesion, ACS Appl. Mater. Interfaces 2 (11) (2010) 3100–3110.
[71] Z. He, E.T. Vågenes, C. Delabahan, J. He, Z. Zhang, Room temperature characteristics of polymer-based low ice adhesion surfaces, Sci. Rep. 7 (1) (2017) 1–7.
[72] M.P. Brenner, D. Lohse, Dynamic equilibrium mechanism for surface nanobubble stabilization, Phys. Rev. Lett. 101 (21) (2008), 214505.
[73] H. Peng, G.R. Birkett, A.V. Nguyen, Origin of interfacial nanoscopic gaseous domains and formation of dense gas layer at hydrophobic solid–water interface, Langmuir 29 (49) (2013) 15266–15274.
[74] X. Zhang, D.Y. Chan, D. Wang, N. Maeda, Stability of interfacial nanobubbles, Langmuir 29 (4) (2013) 1017–1023.
[75] B.H. Tan, H. An, C.-D. Ohl, Stability of surface and bulk nanobubbles, Curr. Opin. Colloid Interface Sci. 53 (2021), 101428.
[76] D. Li, J. Gu, Estimating the Pinning Force of Surface Nanobubbles Based on Trapped Nanobubble Protruding, The Journal of Physical Chemistry C 126 (6) (2022) 3221–3226.
[77] X. Chen, Y. Wu, B. Su, J. Wang, Y. Song, L. Jiang, Terminating marine methane bubbles by superhydrophobic sponges, Adv. Mater. 24 (43) (2012) 5884–5889.
[78] R. Ma, J. Wang, Z. Yang, M. Liu, J. Zhang, L. Jiang, Bioinspired gas bubble spontaneous and directional transportation effects in an aqueous medium, Adv. Mater. 27 (14) (2015) 2384–2389.
[79] S. Li, Y. Hou, M. Kappl, W. Steffen, J. Liu, H.J. Butt, Vapor Lubrication for Reducing Water and Ice Adhesion on Poly (dimethylsiloxane) Brushes, Adv. Mater. 2203242 (2022).
[80] Z. He, Z. Zhang, J. He, CuO/Cu based superhydrophobic and self-cleaning surfaces, Scr. Mater. 118 (2016) 60–64.
[81] E.K. Sam, D.K. Sam, X. Lv, B. Liu, X. Xiao, S. Gong, W. Yu, J. Chen, J. Liu, Recent development in the fabrication of self-healing superhydrophobic surfaces, Chem. Eng. J. 373 (2019) 531–546.
[82] S. Parvate, P. Dixit, S. Chattopadhyay, Superhydrophobic surfaces: insights from theory and experiment, J. Phys. Chem. B 124 (8) (2020) 1323–1360.
[83] S. Jia, X. Lu, S. Luo, Y. Qing, N. Yan, Y. Wu, Efficiently texturing hierarchical epoxy layer for smart superhydrophobic surfaces with excellent durability and exceptional stability exposed to fire, Chem. Eng. J. 348 (2018) 212–223.
[84] C. Zhang, F. Liang, W. Zhang, H. Liu, M. Ge, Y. Zhang, J. Dai, H. Wang, G. Xing, Y. Lai, Constructing mechanochemical durable and self-healing superhydrophobic surfaces, ACS Omega 5 (2) (2020) 986–994.
[85] Y.-Y. Quan, Z. Chen, Y. Lai, Z.-S. Huang, H. Li, Recent advances in fabricating durable superhydrophobic surfaces: a review in the aspects of structures and materials, Mater. Chem. Front. 5 (4) (2021) 1655–1682.